Influence of growth velocity on fragmentation during directional solidification of Al-14 wt.% Sn alloy studied by in-situ synchrotron X-radiography

L. Abou-Khalil, K. Sabat da Cruz, Guillaume Reinhart, N. Mangelinck-Noël, H. Nguyen-Thi

Influence of growth velocity on fragmentation during directional solidification of Al – 14 wt.% Sn alloy studied by in-situ synchrotron X-radiography

L. Abou-Khalil[a*], K. Sabat da Cruz[b], G. Reinhart[a], N. Mangelinck-Noël[a], H. Nguyen-Thi[a]

[a] *Aix Marseille Univ, Université de Toulon, CNRS, IM2NP, Marseille, France.*

[b] *Institute of Engineering and Geosciences - Federal University of the Westside of Pará - UFOPA, CEP: 68035-110, Santarém - Pará - Brazil.*

Abstract:

Directional solidification of Al – 14 wt.% Sn alloy was investigated by means of synchrotron X-radiography at the European Synchrotron Radiation Facility (ESRF). The dynamics of the solidification microstructure formation was studied in-situ and in real-time. In the present manuscript, a special attention is given to the influence of increasing growth velocity on the fragmentation phenomenon of dendrite arms, which has an important role and impact on the final grain structure. Fragmentations of both secondary dendrite arms and more strikingly part of primary trunks have been observed. The experiments show that the number of fragments increases concomitantly with the solidification growth rate until it reaches a limit value after which fewer or no more fragments are observed. The possible origins of the fragmentation are discussed in detail and the likelihood of each of these potential mechanisms is estimated to understand the reason of both primary and secondary arm detachment. It is shown that the fragmentation in a transient regime is correlated to the variations of the solute accumulation, latent heat rejection and the curvature of the attachment neck during solidification. Moreover, during these experiments, Columnar-to-Equiaxed Transition (CET) induced by the fragmentation phenomenon is observed. The velocity of the dendrite fragments due to the buoyancy force

* Corresponding author at Aix Marseille Univ, Université de Toulon, CNRS, IM2NP, 13397, Marseille, France; Email address: lara.aboukhalil@im2np.fr

is a major parameter to control the CET and our results show that a reverse Equiaxed-to-Columnar Transition can even be observed. Once the growth velocity is of the same order or higher than the fragment flotation velocity, the fragments are trapped within the columnar dendritic microstructure, and CET cannot take place or the equiaxed regime cannot be sustained.

Keywords: Solidification, X-ray imaging, Al-Sn, Dendrites, Fragmentation, CET.

1. Introduction

Solidification of metal alloys generally leads to the formation of microstructures at the solid-liquid interface, like cells and dendrites, which determine to a great extent the final mechanical properties of the elaborated material. It is well established that those microstructures are at the origin of severe micro-segregation, as well as of several defects in castings, ingots and welding like hot tears or freckles.

To obtain a regular and stationary dendritic array, it is mandatory to maintain the growth conditions constant during the whole process, as far as possible. However, even in this case, dendrite fragmentation phenomenon can take place during the solidification process, which can generate segregation, microstructure inhomogeneity and defects. Fragmentation is the process of detachment of secondary or tertiary dendrite arms from the primary trunk, or possibly of the primary trunk itself. This mechanism occurs for example during the casting of steel ingots for which massive fragmentation is observed during solidification in the centre of the ingot where the temperature gradient is approaching zero [1,2]. In non-refined alloy casting, the detachment of dendrite fragments is the mechanism that can explain the Columnar-to-Equiaxed Transition (CET). It is generally thought that CET can happen if the detached fragments are transported by convection/buoyancy force not too far ahead of the columnar front and can grow to block the progress of the columnar front [3,4]. Another industrial example for which dendrite

fragmentation plays a detrimental role is the manufacturing of turbine blades made of Nickel-based superalloys [5]. Indeed, the relationship between dendrite fragmentation and freckle occurrence remains an open question for the specific processes of turbine blade fabrication.

To explain why secondary/tertiary dendrite arms detach from primary trunk during solidification, several mechanisms based on the curvature difference at different parts of dendrite arms have been proposed. One of them is the remelting of the dendrite arm neck because of recalescence during solidification from an undercooled melt [6]. This phenomenon is associated to rapid solidification and it can be at the origin of grain refinement [7,8]. Another mechanism is related to solute effects that cause a curvature-driven remelting. The dendrite arms can remelt during coarsening process due to the Gibbs-Thomson effect [9] or by solute enrichment caused by natural convection [10,11] or forced melt flow [12–14], which modify the equilibrium temperature, thus promoting fragmentation.

Clarifying the underlying mechanisms that induce solutal-driven detachment requires experimental methods that allow in-situ studies of both morphological and solutal aspects. Ruvalcaba *et al.* [10] presented results obtained from directional solidification experiments observed by synchrotron X-radiation microscopy. According to their in-situ observations, the solute enrichment at the neck of the tertiary dendrite branches is produced by the solute-rich melt pushed by buoyancy force that flows through the mushy zone (interdendritic liquid). Liotti *et al.* [13] analysed the dendrite fragmentation in the mushy zone by synchrotron X-ray radiography during the directional solidification of Al-Cu alloys with the application of a pulsed electromagnetic field. The authors confirmed that the main mechanism of the fragmentation and detachment of the dendrite arms is the solute pile-up at the bottom of the dendrite branches causing the re-melting. Zimmermann *et al.* [15] and Shevchenko *et al.* [16] studied the effect of pulling rates combined with different fluid flow on the dendritic microstructure. It was shown that the fragmentation is at the origin of the grain refinement at low solidification velocities

independently of the flow intensity in the melt in a non-refined alloy. When increasing the pulling speed, columnar growth dominates, the number of grains decreases, and the mean grain size concomitantly increases in the case of natural convection or of weak intensity forced convection. Oppositely, many equiaxed grains are observed under intense forced flow. These observations are attributed to the competition between the solidification front growth rate and the fluid flow velocity and their effect on the fragment transportation.

Apart from the solutal mechanism, Ananiev *et al.* [17] studied the effect of mechanical loading due to buoyant forces on the solid-liquid interface in thermodynamic equilibrium. They showed that elastic energy can lead to what they called catastrophic elastic remelting of the neck that attaches the secondary arms to the primary trunk and can lead to fragmentation. Indeed, buoyant forces can be at the origin of cumulative bending moments due to the lower moment of inertia there. Secondary arms grow and become heavier and after a certain time the stress is exceeded at the necks, which causes their sudden and irreversible rotation or bending [18]. Frequently, remelting/dissolution of thin solid neck follows arm bending, which results in dendrite fragmentation. The rotation and bending effects have also been analysed by Reinhart *et al.* [19] and Jung *et al.* [20] during the solidification of Al – 7 wt.% Si. Furthermore, Salloum-Abou-Jaoude *et al.* [21] underlined the major impact of gravity on the fragmentation phenomenon, as well as on the movement of fragments in Al – 20 wt.% Cu by performing a comparison between solidification experiments carried out on Earth and in microgravity. In a review paper, Akamatsu *et al.* [22] reported dramatic difference of fragmentation density between experiments carried out in microgravity conditions, without buoyancy force and fluid flow, and under normal conditions. They concluded that the fragmentation is most likely not a purely diffusive process. Cai *et al.* [23] emphasized the impact of buoyancy forces on dendrite fragmentation during vertical upward solidifications of Al – 15wt.% Cu samples via X-ray tomography. The authors concluded that mechanical deformation from various sources may

play a much greater role in grain fragmentation during solidification than previously thought. In a very recent paper, Nelson *et al.* [24] found a marked difference in fragmentation density between vertical upward and downward solidification for the same alloys. They attributed this to the change of buoyancy force that modulates the solute flow convection and that stresses the dendrite arms.

The fragmentation during directional solidification of Al – 14wt.% Sn alloys is the subject of the present work. Al-Sn alloys are well known for having excellent tribological [25] and mechanical properties, making this kind of system suitable for the application in combustion engine pistons and cylinder liners [26]. The origin of their outstanding properties relies on the Sn particles spread over a continuous Al-rich matrix. The tough Al-rich matrix, which is more resistant to high mechanical loads, works in combination with the Sn particles that act as solid lubricants. The experiments presented in this paper were carried out at the European Synchrotron Radiation Facility (ESRF) where in-situ X-radiography technique was used to reveal the dynamics of grain structure formation with a particular focus on fragmentation and on CET induced by fragmentation. The solidification was achieved in a transient condition that is similar to industrial casting processes such as direct-chill casting [27], with the concomitant increase of growth velocity and decrease of temperature gradient. This allows a better understanding of the fragmentation phenomenon during the elaboration of the industrial material and its effect on the final structure [4,20]. Several mechanisms at the origin of fragmentation are discussed in details as well as the impact on the resulting microstructure and grain structure.

2. Experiments

Directional solidification experiments were carried out on beamline ID19 at ESRF (Grenoble, France) in a Bridgman furnace set-up previously described in detail in [28,29]. The nominal alloy composition was Al – 14 wt.% Sn. The sample dimensions were 40 mm in length, 5 mm in width and about 300 µm in thickness. It was sandwiched between two graphite foils and two molybdenum diaphragms, held together with two clips and fixed to a sample holder. The whole assembly was then inserted vertically into the Bridgman furnace placed in a high vacuum chamber (Fig.1).

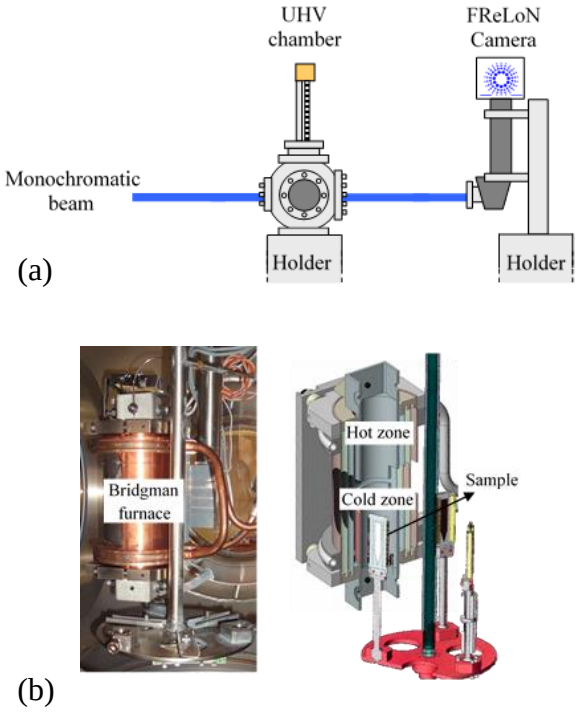

Figure 1: (a) Sketch of in-situ synchrotron X-ray imaging setup. (b) Picture and 3D drawing of Bridgman furnace.

The temperatures of the top and bottom zones of the furnace were first adjusted to achieve the desired initial temperature gradient G_i (Table 1). The temperature gradient was applied between the two heater elements regulated by two embedded K-type thermocouples 4.5 cm

apart. Then, solidification was triggered by cooling only the top heater of the furnace (R_T) while maintaining the bottom heater temperature constant, with displacement of neither the sample nor the furnace. The application of a cooling rate only on the top heater induced a progressive decrease of the temperature gradient in the sample, similar to industrial casting conditions, for example direct-chill casting [27]. For all experiments, an initial transient period was observed. After a while, the decrease of the temperature gradient became linear. The values of the temperature gradient variation with respect to time ($\dot{G}$) are given in Table 1. The observation and analysis of experiments were performed during the period of linear decrease of the temperature gradient.

Table1: Experimental parameters; R_T is the cooling rate applied to the top heater element. The temperature of the bottom heater element is maintained constant. G_i and G_f are the initial and final temperature gradients, respectively. $\dot{G}$ is the temperature gradient variations with respect to time.

Experiments	**R_T (K/min)**	**G_i (K/cm)**	**G_f (K/cm)**	**$\dot{G}$ (K /cm/min)**
(A)	0.2	22.4	10.6	-0.04
(B)	0.5	26.0	14.1	-0.11
(C)	8.0	23.7	15.3	-1.70
(D)	16	22.6	17.0	-2.44

The availability of high energy X-rays in synchrotron accelerators allows the emergence of characterization methods than can be applied to the study of solidification microstructure formation of metallic alloys [30,31]. In this paper, synchrotron X-radiography was used to investigate the dynamics of the microstructure formation during solidification and solute distribution in the melt. This technique is based on the local changes in the amplitude of a transmitted X-ray beam due to differential absorption by an inhomogeneous sample [32,33]. In Al-based alloys, contrast firstly results from segregation of the chemical species and secondly from the difference of density between the solid and liquid phases. X-radiography enables us

to follow the dynamics of the solid-liquid interface [33], the grain motion [21,34,35] and under certain conditions to determine quantitatively the solute concentration in the liquid phase [36,37]. In our experiments, the main surface of the sample (40 x 5 mm) was perpendicular to the horizontal incident monochromatic X-ray beam with an energy of 14 keV. The Fast Readout–Low Noise (FReLoN) CCD camera developed at ESRF was used as detector and the camera optics were chosen to obtain a good compromise between a large field of view (14 mm x 6 mm) and a suitable spatial resolution (pixel size 7.46 x 7.46 μm^2). The high intensity of synchrotron radiation makes it possible to record images with enough contrast. Images were recorded with different exposure time (0.5 to 4 s) and time intervals (1 to 14 s) depending on the solidification velocity and on the phenomena of interest.

For the experiments presented in this paper, successive images of the solid-liquid zone were recorded during the whole solidification step, and it was thus possible to display videos of the time evolution of the solid-liquid interface. Image processing was applied to improve the quality of the radiographs, which consisted in dividing the raw images of the sample taken at time t during solidification by a reference image. This reference image was recorded just before cooling down started, when the sample was mostly liquid and homogeneous with a constant initial solute concentration C_0 [36]. The result was an enhanced contrast and a defect-free image. In these images, the Al-dendrites that have a lower density relatively to the Sn-enriched liquid appear in white or light grey and Sn-enriched liquid in dark grey.

3. Results

3.1. In-situ investigation of the microstructure evolution/interface destabilization

Figures 2 and 3 display two sequences of radiographs showing the evolution of solidification microstructures of Al – 14 wt.% Sn alloy, at a very slow cooling rate of 0.2 K/min and 0.5 K/min on the top heater element, respectively. Radiographs show that Al-Sn samples

did not keep their initial rectangular shape and were deformed during the melting phase.

At the early stages of the cooling process, the initial solid-liquid interface is smooth and inclined (Fig.2a), most likely due to a residual transverse temperature or solutal gradients. As solidification proceeds, the gradual decrease of the longitudinal temperature gradient augments the instability level of the solid-liquid interface, so that a transition from a planar to cellular front occurs after few minutes of the cooling process, and a dendritic microstructure is formed on both sides of the sample (Fig.2b and Fig.3a,b). The dendritic pattern then spreads towards the centre of the solid-liquid interface until the whole interface become dendritic. As the sample cooling continues, the formation of developed microstructures with more branches that become more pronounced is observed (Fig.4).

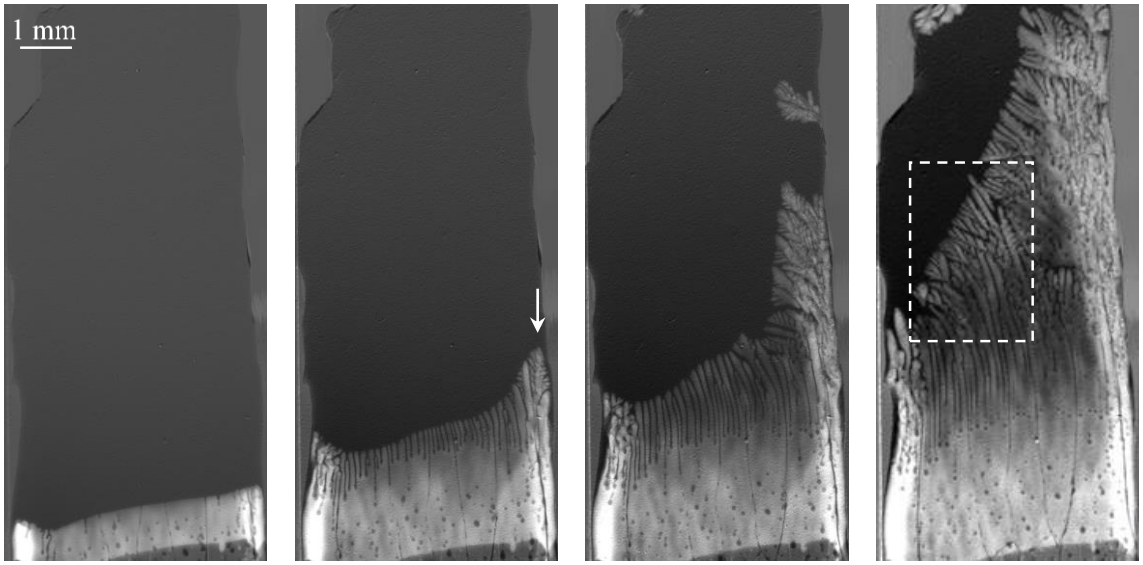

(a) t = 79.2 min (b) t = 148.5 min (c) t = 185 min (d) t = 250 min

Figure 2: Sequence of radiographs showing the evolution of the solidification microstructure of Al – 14 wt.% Sn by applying a cooling rate of R_T = 0.2 K/min on the top heater element only. The white arrow points to the dendrite whose growth rate evolution is plotted in Figure 5a. A close-up of the growth of the microstructure growth inside the dashed white zone is shown in Figure 4a (top). (See supplementary material for the corresponding movie).

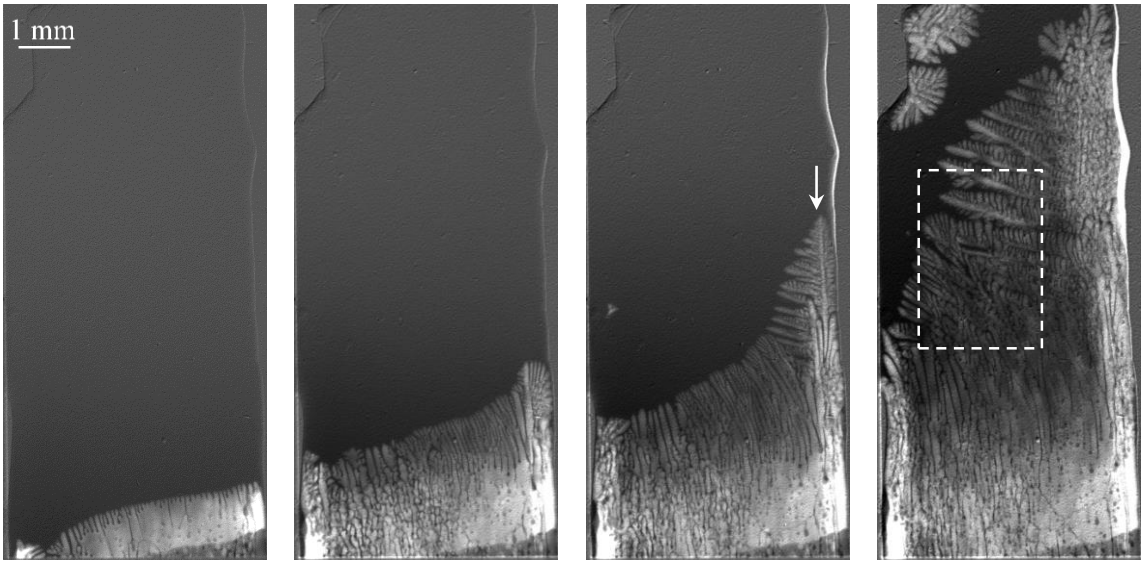

(a) t = 36.3 min (b) t = 62 min (c) t = 74.1 min (d) t = 102.8 min

Figure 3: Sequence of radiographs showing the dynamics of the solid-liquid interface during the solidification of Al – 14 wt.% Sn by applying a cooling rate of R_T = 0.5 K/min on the top heater element only. The white arrow points to the dendrite whose growth rate is plotted in Figure 5b. A close-up of the growth of the microstructure growth inside the dashed white zone is shown in Figure 4b (bottom). (See supplementary material for the corresponding movie).

(a) R_T = 0.2 K/min

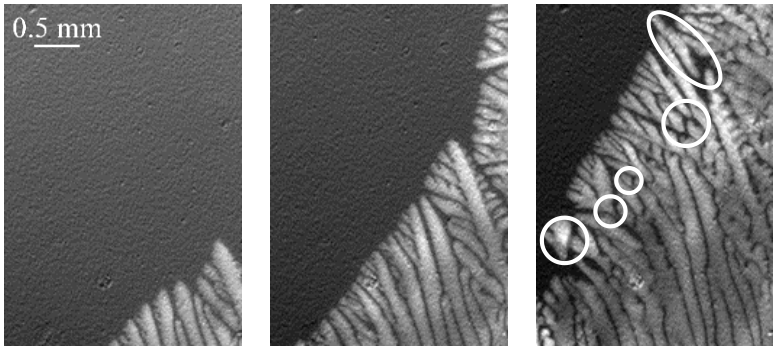

(a_1) t = 200.2 min (a_2) t = 219.4 min (a_3) t = 248.6 min

(b) R_T = 0.5 K/min

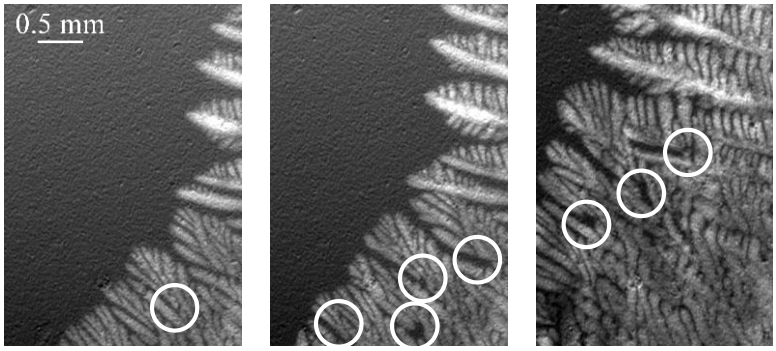

(b_1) t = 86 min (b_2) t = 89.4 min (b_3) t = 103 min

Figure 4: Sequence of radiographs showing the evolution of the microstructure and the dendrite branching inside the white dashed zones in Figures 2 and 3 solidified by applying a cooling rate of R_T = 0.2 K/min and 0.5 K/min on the top heater element only, respectively. The white circles represent the location of some of the dendrite fragments.

The dendrite growth velocities of the two far right dendrites in Figures 2 and 3 are measured from the radiographs and are plotted in the graphs in Figure 5. As expected, the growth velocity increases during the experiment as solidification is achieved by cooling only the top heater of the furnace while maintaining the bottom heater temperature constant. The growth rate increases, from ~ 1.2 µm/s to ~ 3 µm/s for the experiment solidified at R_T = 0.2 K/min and from ~ 4 µm/s to ~ 11 µm/s for the experiment solidified at R_T = 0.5 K/min.

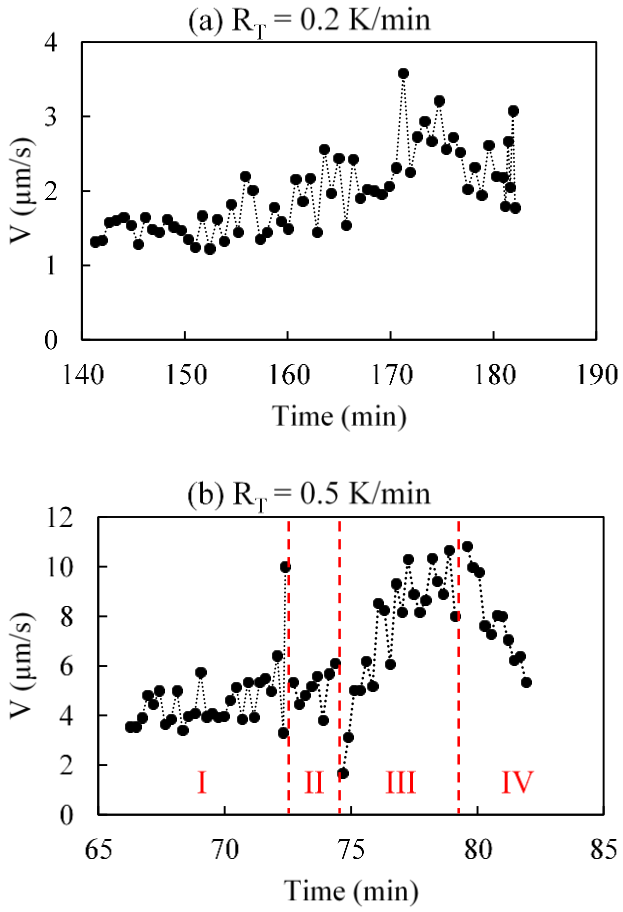

Figure 5: Tip growth rate as a function of time of the two far-right dendrites (pointed by white arrows) for the experiments solidified by applying (a) R_T = 0.2 K/min (in Figure 2) and (b) R_T = 0.5 K/min (in Figure 3). The red dashes indicate when the dendrite detachments occur.

3.2. In-situ investigation of fragmentation

In the experiments solidified at cooling rates R_T = 0.2 K/min and R_T = 0.5 K/min, the first fragmentation phenomena are surprisingly observed during the cellular growth for a growth velocity larger than ~ 1.7 µm/s; below this value no fragment is detected. The detachment of few cells is observed directly by in situ X-radiography for the first time to the best of our knowledge (Fig.6). In Figure.6b, the cell to dendrite transition occurs with the development of some secondary arms in the sample thickness.

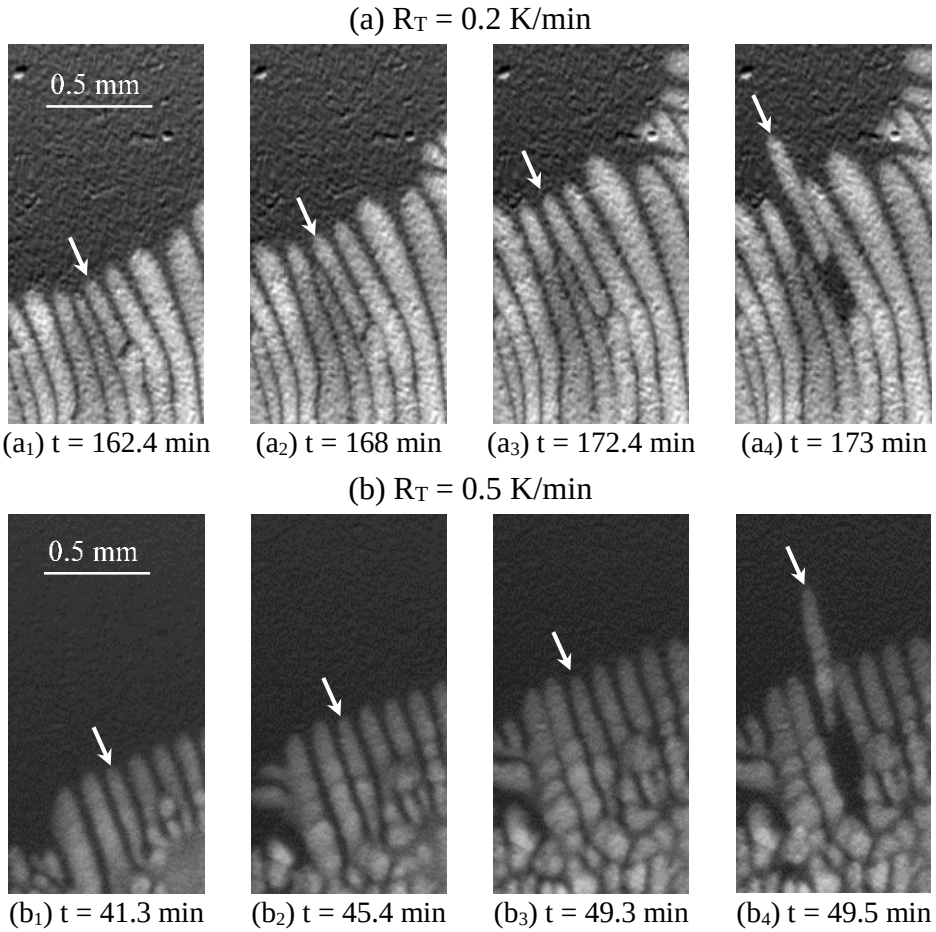

Figure 6: Sequence of radiographs, taken from the experiments solidified by applying a cooling rate of (a) R_T = 0.2 K/min and (b) 0.5 K/min on the top heater element only, showing the evolution of cell neck shape and size before its detachment.

At a later stage, following the development of the dendritic microstructure, several detachments of dendritic branches occur during the two experiments. As the growth velocity increases, the number of fragments also increases progressively. Additionally, during the dendrite development, secondary dendrite arm bending is repeatedly observed and generally followed by detachment. They rotate around their neck in the upward direction by 3° to 7° and then detach (Fig.7). Moreover, a repetitive and somewhat unexpected phenomenon in these experiments is the fragmentation of the primary dendrite trunks (Fig.2c, Fig.3c and Fig.7). By using in-situ observation, the detached fragment behaviour is followed in detail. The free fragments, i.e., not blocked inside the mushy zone, float towards the top region (i.e., towards higher temperatures) and melt while others get stuck in the thickness of the sample and continue to grow locally (see supplementary materials).

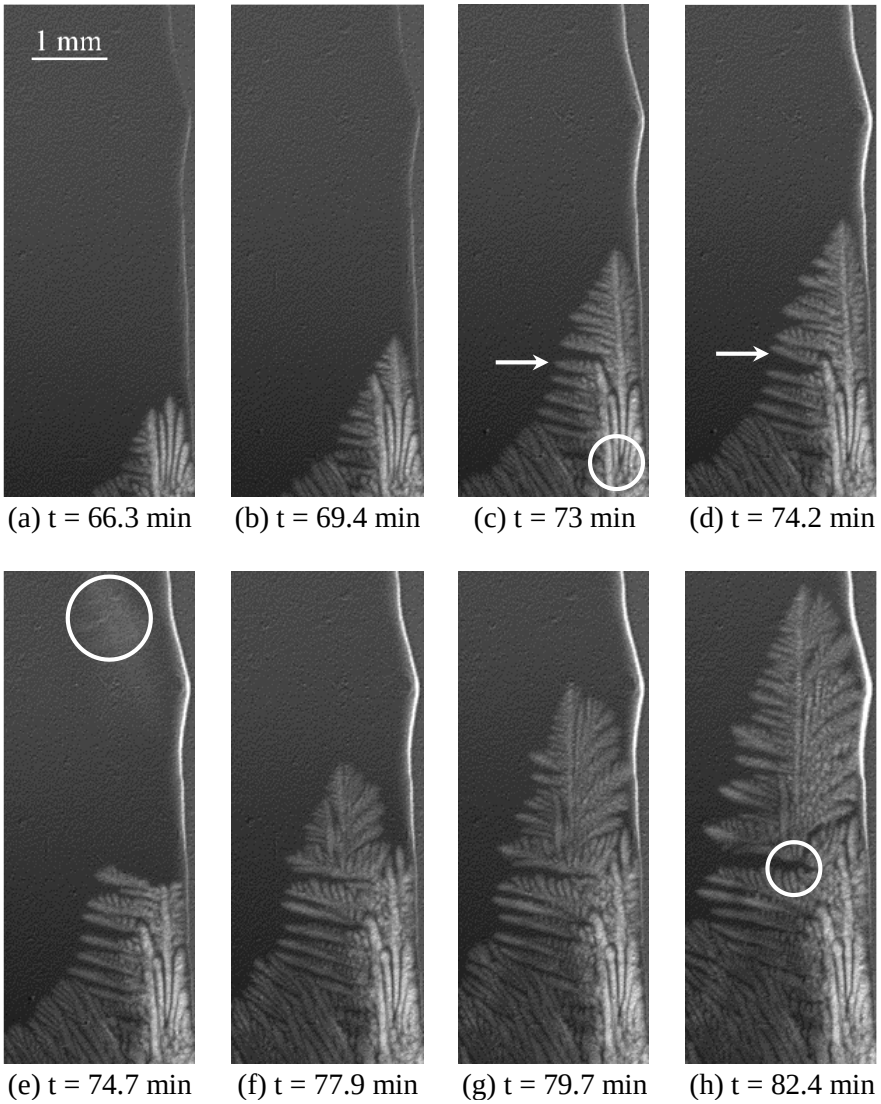

Figure 7: Sequence of radiographs showing the dynamics of the far-right dendrite pointed by a white arrow in Figure 2. The detachments of the primary trunk are highlighted by white circles. The white arrows showing the position of the secondary arm before and after bending.

A remarkable example of the phenomena observed in our experiments is the dynamics of the far-right dendrite in Figure 2, which is initially a tertiary arm. The behaviour of this dendrite is presented in Figure 7 and described in detail in the following. First, its growth velocity increases from ~ 4 µm/s to ~ 10 µm/s with a maximum of growth rate just before its first detachment (Fig.7a,b and region I in Fig.5b). The broken primary branch (white circle in Fig.7c) stands close to its initial position and starts growing again. The upward bending of some secondary arms is observed (Fig.7c,d). Several seconds later, a new maximum value of the growth velocity is reached (~ 4.5 µm/s to ~ 6 µm/s) for the tip of the far-right dendrite and a

new detachment of the primary trunk occurs (region II in Fig.5b). This fragment floats and melts while reaching the hot region of the sample (Fig.7e). A tertiary arm takes over and grows (Fig.7f). Its growth rate first decelerates under the effect of the melted fragment, then it accelerates (region III in Fig.5b), and the tertiary arm continues its growth along the direction of the temperature gradient as a primary trunk (~ 1.6 µm/s to ~ 10.6 µm/s). Then, a bending of the secondary arm from which this tertiary arm started occurs (Fig.7g and region IV in Fig.5b). Consequently, the tip of the tertiary arm moves slightly upward in a liquid region with a lower solute concentration. A deceleration of the tertiary arm growth follows, which is probably due to the time necessary to recreate a solutal layer in front of the tip. Few minutes later, the secondary arm with its corresponding tertiary arm detaches, the fragment is blocked and continues its growth (Fig.7h).

It is worth noticing that the final structure of the sample solidified at 0.2 K/min and 0.5 K/min appears columnar with no clear evidence of the fragmentation history except for the indirect effect of the fragmentation that induces dendrite disorientations from the initial growth direction (Fig.2d and Fig.3d).

3.3. Columnar-to-Equiaxed Transition (CET) by fragmentation

Figures 8 and 9 show the microstructure evolution of Al – 14 wt.% Sn solidified at higher cooling rates of 8 K/min and 16 K/min on the top heating zone, respectively. For these higher cooling rate values, the solid-liquid interface becomes rapidly dendritic after the application of the cooling. Concomitantly, a lot of fragmentations of primary, secondary and tertiary branches are observed (Fig.8a, Fig.9a).

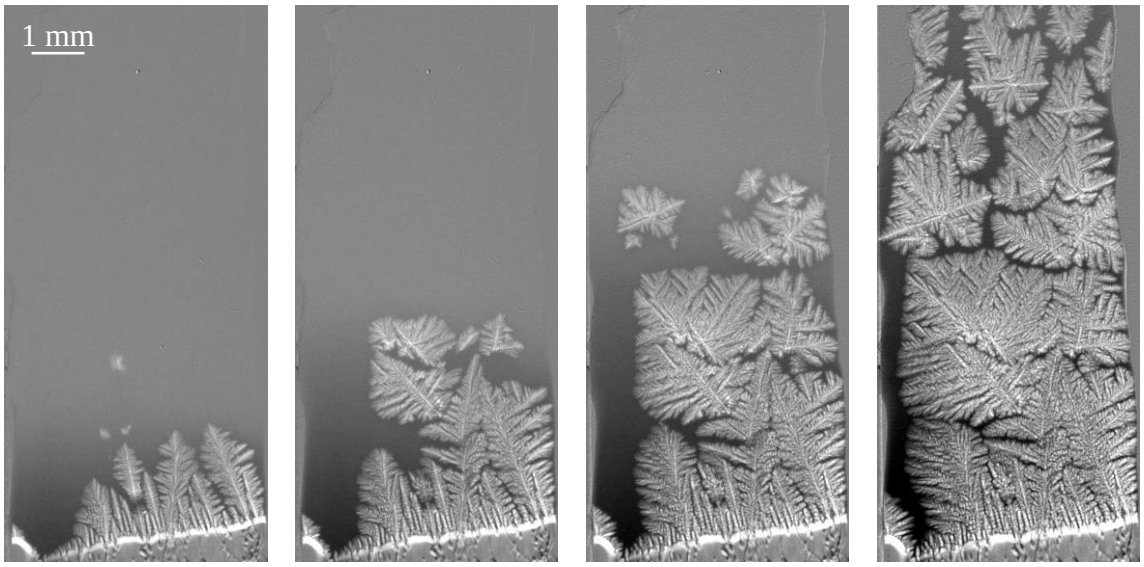

(a) t = 3.6 min (b) t = 4.5 min (c) t = 5.4 min (d) t = 6.7 min

Figure 8: Sequence of radiographs showing the Columnar-to-Equiaxed Transition due to the fragmentation during the solidification of Al – 14 wt.% Sn by applying a cooling rate of R_T = 8 K/min on the top heater element only. (See supplementary material for the corresponding movie).

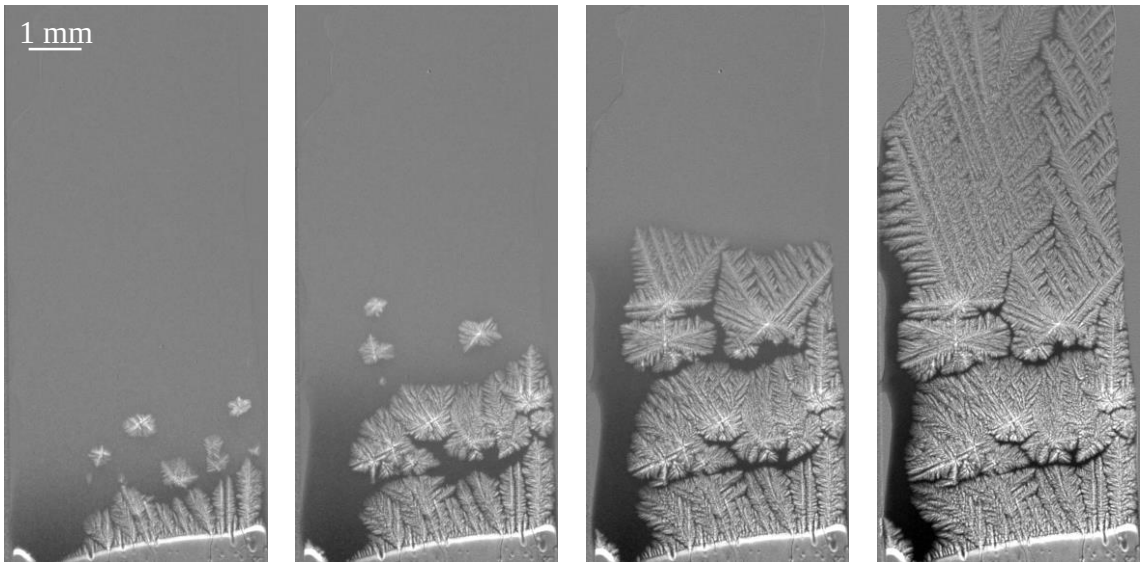

(a) t = 1.6 min (b) t = 2.1 min (c) t = 2.6 min (d) t = 3.3 min

Figure 9: Sequence of radiographs showing the Equiaxed-to-Columnar Transition during the solidification of Al – 14 wt.% Sn by applying a cooling rate of R_T = 16 K/min on the top heater element only. (See supplementary material for the corresponding movie).

In the experiment solidified at R_T = 8 K/min, some fragments float and melt once they reach the hot region while the others are blocked during their flotation and continue to grow locally forming a layer of equiaxed grains that blocks the initial columnar front (Fig.8a,b). The

equiaxed grains develop and become more and more elongated. Then, new fragmentations occur, and new grains are blocked in the thickness. This process is repeated causing successive Columnar-to-Equiaxed Transitions (Fig.8c). The final grain structure is composed of several layers of packed elongated grains either connected or separated by a Sn-rich segregated band (Fig.8d).

For the experiment performed at R_T = 16 K/min, the same microstructure behaviour is observed in the beginning where one layer of elongated grains is formed that blocks the initial columnar front, then two fragments from this first layer are blocked above the interface (Fig.9a,b). Contrary to the previous experiment, at the end, a columnar front develops from the solidification front without any further fragmentation (Fig.9c). Therefore, an Equiaxed-to-Columnar Transition is observed (Fig.9d). It is worth noticing that fragmentation phenomena are mainly observed inside the mushy zone in both samples during the coarsening step.

4. Discussion

The most important observation in these experiments is the great number of fragmentation events of secondary, tertiary and even primary arms during the sample cooling. As seen in the introduction, several mechanisms can be at the origin of dendrite detachment such as mechanical and solutal effects. These effects will be discussed in detail in this section, as well as the consequence of fragmentation on the final grain structure.

4.1. Effect of growth velocity on microstructure evolution

In the case of Al – 14 wt.% Sn alloy, most of solute is rejected during the liquid to solid transformation because of the value of the partition coefficient $k \approx 0.033$ which is well below unity. As the solute (Sn) is denser than the solvent, it accumulates in the melt ahead of the solid-liquid interface. This solute layer induces a constitutional undercooled region, which is at the origin of the solid-liquid interface instability and the formation of cellular or dendritic patterns

[38,39]. Interface destabilisation depends on the temperature gradient (G), growth velocity (V) or cooling rate and alloy concentration. The change in the interface morphology is controlled by the ratio G/V, where the solid-liquid interface tends to be dendritic when the ratio is small (small temperature gradient or high growth rate) [40]. In the experiments presented in this article, the solidification occurs in transient conditions because of the gradual decrease of the temperature gradient and the progressive increase of the growth velocity as shown in Figure 5. Accordingly, the ratio G/V gradually slows down, which leads to the breakdown of the planar solidification front to give cells and then, dendrites. In the case of the experiments with the highest cooling rates applied on the top heater (8 and 16 K/min), the cellular pattern is skipped and the solid-liquid interface is dendritic from the very early stages of solidification (see Fig.8 and Fig.9 and corresponding videos in the supplementary material).

The initial inclination of the solid-liquid interface observed for all experiments (Fig.2a, Fig.3a, Fig.8a and Fig.9a) is caused by a transverse temperature gradient in the sample and worsened due to the shape of the sample. This transverse temperature gradient induces a transverse convective flow. Consequently, the solute concentration varies along the solid-liquid interface from one side to the other. Solute accumulates in depressed regions, which modifies locally the equilibrium temperature, and leads to the delay in the growth on the left side and to the dendrite formation on the right side (Fig.2b, Fig.3b) [31]. Those two effects amplify throughout the growth process.

The growth velocity also affects the dendrite dimensions. As the growth rate increases, the microstructure becomes finer: a reduction in the diameter size of the dendrite arm is observed and a decrease of the secondary arm spacing is detected [41]. As an example, in the experiment where the applied cooling rate is R_T = 0.5 K/min, the secondary arm spacing of the right dendrite decreases from ~ 200 µm to ~ 100 µm and a lot of ramifications occurs as shown in Figure 4 due to the progressive increase of the growth rate.

4.2. Impact of mechanical effect

4.2.1. Mechanical effect on primary trunks

During the solidification of Al – 14 wt.% Sn, the detachment of primary trunks growing parallel to the temperature gradient direction is observed. In Al-Sn alloy, the density of the formed solid (ρ_S = 2585 kg/m^3) is lower than the density of the surrounding liquid (ρ_L = 2617 kg/m^3) so that the buoyancy force exerted on the solid is upward like in Al-20wt%Cu alloys [42] and contrary to Al-Si and Al-Ni alloys where this force is exerted downwardly [19,43]. A model was proposed by R.H. Mathiesen *et al.* [11,44] to determine the limit thickness of the primary arm neck for which the deformation of the neck is plastic and thus can lead to fragmentation by a mechanical effect. In this model, the potential fragment is assimilated to a sphere with an equivalent radius R_e and a neck radius r (Fig.10). The detachment takes place when $R_e$exceeds a value given by the equation 2:

$$R_e > \left(\frac{2\sigma_B}{4\Delta\rho g} r^2\right)^{1/3} \quad (2)$$

with σ_b the critical stress, and $\Delta\rho$ the density difference between liquid and solid phases.

From equation (2), it is possible to determine the minimum value range of primary arm neck radii for which the deformation is plastic. We impose a value range of Re from 50 µm to 150 µm (keeping in mind that the thickness of the sample is 300 µm) and σ_B = 0.14 MPa for aluminium [43]. According to this model, the calculated range of the neck radius is ~ 0.02 µm < r < 0.12 µm, which means that the neck radius must be as small as these values to obtain detachment due solely to mechanical effect.

However, in our experiments, the dendrite arm neck of the growing microstructures is much larger (micrometers to tens of micrometers). Therefore, it can be concluded that buoyancy force alone is not sufficient to provoke fragmentation of primary trunks. This result is in agreement with B. Cai *et al.* [23] work, where they proposed that buoyancy induced mechanical effect is

too small to cause the fragmentation without additional mechanisms. Mechanisms at the origin of the neck arm pinch-off and so of subsequent dendrite arm fragmentation will be discussed in the following.

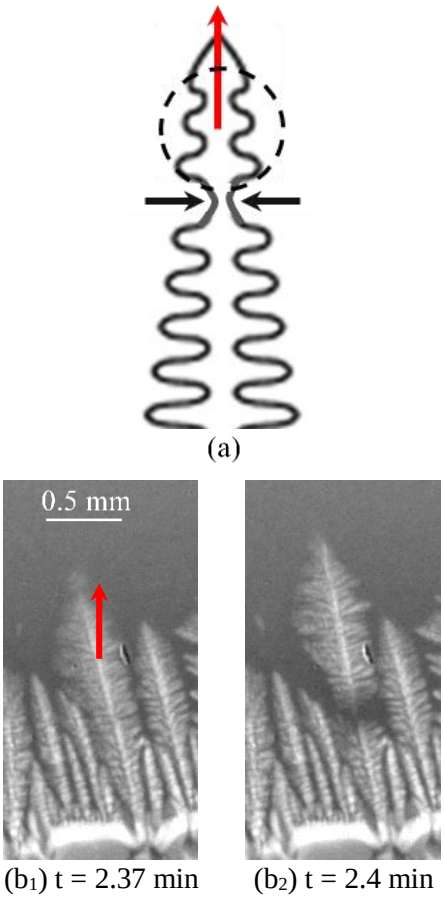

(a)

(b_1) t = 2.37 min (b_2) t = 2.4 min

Figure 10: (a) Sketch illustrating the irreversible neck deformation of the primary trunk under the buoyancy force leading to the detachment of the top of the dendrite. The potential fragment is assimilated to a sphere with an equivalent radius Re and a neck radius r. (b) Two consecutive radiographs from experiment (D) solidified at R_T = 16 K/min, showing the detachment of a primary trunk.

4.2.2. Upward bending of secondary arms

The radiographs in Figure 11b and 11c show the upward bending and detachment of two secondary arms. These pictures are obtained after an image processing named frame differencing, which consists in dividing a radiograph by a previous one. The positions of the secondary arms before bending are illustrated in black and their new positions in white. The

cause of the bending is linked again to density difference between liquid and solid phases, which is at the origin of an upward buoyancy force. Reinhart *et al.*[43] analysed the mechanical stresses that are localized at the thin solid necks that attach the secondary arms to the primary trunk. They showed that the mechanical stresses accumulate there as the arms grow. Subsequently, the yield stress can be exceeded at the necks, which causes their sudden and irreversible rotation as presented in Figure 11. Secondary arm detachment is observed all along the solidification experiments and sometimes follows dendrite bending. However, using the same argument as in section 4.2.1, it can be concluded that the buoyancy force is not sufficient to provoke fragmentation alone. In our previous work, detachment of secondary arms is also observed in Al – 7wt.% Si following dendrite bending [19] although due to a reverse solid and liquid ratio, the bending is observed in the downward direction.

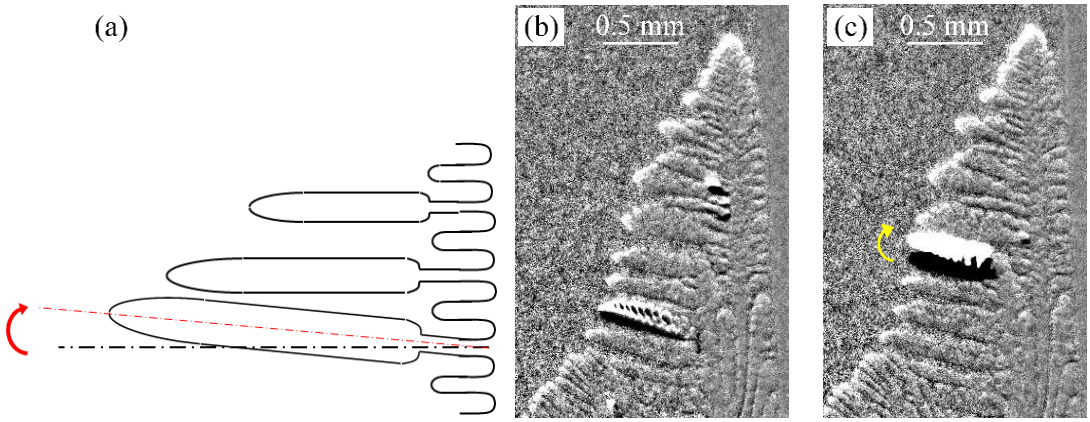

Figure 11: (a) Sketch depicting the upward bending of a secondary arm due to buoyancy force. (b) and (c) two pictures showing the bending of two different secondary arms during experiment (B) solidified at R_T = 0.5 K/min. These pictures are obtained by an image processing (frame differencing), the positions of the secondary arms before and after upward bending appear respectively in black and in white.

4.3. Origin of fragmentation

The microstructure formation in the experiments presented in this work takes place in a transient regime. Decreasing the temperature gradient progressively induces a gradual increase of the dendrite growth velocity (Fig.5), which is accompanied by a continuous increase of the

solute and latent heat rejection. The solute is transported from the cell/dendrite tips toward their roots as it is denser than the solvent. The solute accumulation around the microstructure, together with the heat rejection, modify locally the temperature and restrict the neck growth which leads to its size reduction and can ultimately contribute to its detachment as pointed out by Ruvalcaba *et al.* [10]. The solute concentration was measured locally at some detachment points by applying the image processing presented in A. Buffet et al. [36], where the grey scale of the radiographs was converted to solute concentration. The fragmentation occurs for an enrichment of 20 – 25 wt.% Sn in the beginning and then later during solidification the concentration increases further to reach 30 wt.% Sn. As shown in Figure 6, the detached cells already represent small radii that reduce respectively during the growth due to the solute accumulation which leads to their detachment.

Moreover, an important feature to mention is that several fragmentation phenomena are preceded by a sudden increase of the growth rate (Fig.5), which goes with increased local solute and heat rejection. However, during the directional solidification of transparent alloys, Liu *et al.* [45] showed that under sharp decreasing growth rate, the arm detachment is accelerated due to the rising of interdentritic solute concentration that induces the dissolution of narrow attachment necks of the primary stems. This observation confirms that fragmentation is correlated to the variations during solidification of the local columnar tip growth rates, to the curvature of the attachment necks and to the geometrical arrangement of neighbour dendrites. So, it seems that the transient conditions applied in the present work enhance the fragmentation phenomenon.

Some detached fragments can also contribute to further fragmentation as can be seen in experiments (C) and (D) solidified at R_T = 8 K/min and 16 K/min, respectively (see supplementary materials). As the fragments float, they can melt or grow and thus reject solute that is transported by the flow toward the mushy zone and provokes the melting of other necks

that can induce new fragmentation events [10,11].

Moreover, as discussed in section 4.1, the dendritic microstructure evolution strongly depends on the growth velocity and this evolution can make the microstructure more prone to fragmentation. Indeed, because of the progressive increase of the growth rate, the microstructure becomes finer and shows several successive ramifications (Fig.4). The attachment necks of these new branches are already thin, which makes them easy to detach. In most cases, fragmentation occurs after several successive branching and thus in the case of finer dendrites (Fig.4). In fact, some detached primary trunks are initially tertiary branches (Fig.7). The fact that the structure becomes finer [41] during the growth process can facilitate the fragmentation. H. Neumann-Heyme *et al.* [46] showed that if the secondary arm spacing (λ_2) is large, the solidification effect is predominant compared to the capillarity effect (coarsening). Oppositely, the tendency for pinch-off (detachment) is enhanced for smaller λ_2 (finer structure).

Adding to the above effects, the mechanical effect can also contribute to the detachment processing in Al-Sn alloy when the buoyancy force is acting upwardly; either by the stretching of the arms or of parts of the primary trunks which can reduce the neck radius and facilitate the fragmentation due to the mechanisms described above.

4.4. Effect of the fragmentation on the final grain structure and CET

The final microstructure is strongly related to the growth velocity and to the fragmentation phenomenon that occur during the solidification process. In the experiments solidified at the lowest cooling rates R_T = 0.2 K/min and R_T = 0.5 K/min (Fig.2d, Fig.3d), the final microstructure is columnar with a segregated channel due to the convective flow with no clear traces of fragmentation when looking at the final grain structure. Without the in-situ investigation, the fragment dynamics could not be detected in detail from the final structure. No direct impact of fragmentation on the final structure is observed but it does affect the dendrite crystallographic orientation, especially when the fragments rotate while floating or due

to the small fragments that are detached inside the mushy zone during the coarsening.

The final grain structure of the sample solidified at R_T = 8 K/min is composed of successive layers of elongated equiaxed grains (Fig.8d) either connected due to the coalescence and coarsening phenomena or separated by a Sn-rich segregated band. These equiaxed grains are initially fragments that are blocked above the solid-liquid interface and continue their growth whereas the ones that go in the upper part of the sample are remelted. In our experiments, the fragment floatation is hindered due to the thin samples. However, it can also occur in bulk ingots when a high amount of fragments are competing with each other and stop the growth of the columnar front [4].

Each new layer is due to fragmentations from the grains below. So, the fragmentation can produce a Columnar-to-Equiaxed Transition grain structure that is repeatedly observed during solidification even in this non-refined alloy and at a relatively low cooling rate.

As seen in the result section 3.3, CET is also observed (Fig.9a,b) at the beginning of the experiment solidified at the highest cooling rate (R_T = 16 K/min). As a second step, columnar growth starting from the second layer of equiaxed grains is characterised. The growth rate of the solidification front is compared to the floating velocity of fragments to understand these transitions. From the beginning of the solidification, detachment of dendritic branches is observed, they float toward the hot zone with a velocity of ~ 100 µm/s to ~ 200 µm/s while the growth rate of the interface is increasing from ~ 35 µm/s to ~ 60 µm/s. As long as the solidification velocity is lower than the fragment floating velocity, the fragments have enough time to leave the interface and to move up due to the buoyancy force. As a first step and similarly to experiment (C), a layer of elongated equiaxed grains issued from fragmentation develops above the columnar front so that a Columnar-to-Equiaxed Transition is observed. A second layer is formed by the same mechanism. However, as soon as the growth velocity reaches the floating fragment velocity, the fragments are trapped because the buoyancy force is

not sufficient to bring them out from the solidification interface. As a result, a columnar front dominates and an Equiaxed-to-Columnar Transition is observed (Fig.9d). Thus, there is an optimum of solidification parameters to obtain and maintain CET by fragmentation.

5. Conclusion

Directional solidification of Al – 14 wt.% Sn alloy was investigated by means of synchrotron X-ray radiography imaging techniques. In order to be close to industrial conditions such as direct-chill casting [27], solidification was triggered by simultaneously decreasing the temperature gradient, and increasing the solidification rate. A strong correlation between the growth velocity and the fragmentation phenomenon was demonstrated under transient regime.

The results show that the number of detached secondary, tertiary arms and even primary trunk sections raises gradually by increasing the growth velocity while reducing the temperature gradient. This phenomenon takes place until the growth velocity reaches the fragment floatation velocity so that the fragments cannot anymore escape from the mushy zone.

The mechanical effect induced by the buoyancy force is the cause of the irreversible secondary arms bending and of the deformation of the primary arms size, which can contribute to the fragmentation. However, we show that it cannot be the only mechanism at stake. In fact, increasing the growth velocity is at the origin of the increase of solute and latent heat rejection and of finer and ramified dendrites which make the microstructure more prone to the fragmentation phenomenon by remelting and capillarity effect.

It is also shown that the fragmentation can have a major impact on the final grain structure. It can be at the origin of CET and of an equiaxed grain structure in a non-refined alloy solidified at relative low growth rate for optimum solidification conditions and can create local disorientations within the final grain structure. The CET can take place and the equiaxed regime can be maintained by the fragmentation phenomenon only if the fragment flotation velocity is

higher than the front growth velocity.

6. Supplementary data

Supplementary data related to this article can be found at (link to supplementary material).

7. Acknowledgments

The authors acknowledge financial support provided by CNRS (The Scientific Research foundation from France) and CNPq (The Brazilian Research Council). In addition, the authors would like to thank ESRF (European Synchrotron Radiation Facility) ID19 team for its support during the in-situ experiments.

8. References

[1] B. Gerin, H. Combeau, M. Založnik, I. Poitrault, M. Cherif, Prediction of solidification structures in a 9.8 t steel ingot, IOP Conf. Ser. Mater. Sci. Eng. 529 (2019) 012036. https://doi.org/10.1088/1757-899X/529/1/012036.

[2] H. Combeau, M. Založnik, M. Bedel, Predictive Capabilities of Multiphysics and Multiscale Models in Modeling Solidification of Steel Ingots and DC Casting of Aluminum, JOM. 68 (2016) 2198–2206. https://doi.org/10.1007/s11837-016-1993-z.

[3] H.J. Jung, N. Mangelinck-Noël, H. Nguyen-Thi, N. Bergeon, B. Billia, A. Buffet, J. Baruchel, CET by Fragmentation during the Solidification under Natural and Forced Convection of Non-Refined Al-Based Alloys, Mater. Sci. Forum. 649 (2010) 343–348. https://doi.org/10.4028/www.scientific.net/MSF.649.343.

[4] Ch.-A. Gandin, Experimental Study of the Transition from Constrained to Unconstrained Growth during Directional Solidification., ISIJ Int. 40 (2000) 971–979. https://doi.org/10.2355/isijinternational.40.971.

[5] G. Reinhart, D. Grange, L. Abou-Khalil, N. Mangelinck-Noël, N.T. Niane, V. Maguin, G. Guillemot, Ch.-A. Gandin, H. Nguyen-Thi, Impact of solute flow during directional solidification of a Ni-based alloy: In-situ and real-time X-radiography, Acta Mater. 194 (2020) 68–79. https://doi.org/10.1016/j.actamat.2020.04.003.

[6] Toshihilo Koseki, Flemings Merton C., Effect of extraction on dendritic growth into undercooled melts, ISIJ Int. (1995) 611–617.

[7] A.M. Mullis, N. Haque, Direct observation of dendrite fragmentation in the solidification of undercooled melts, IOP Conf. Ser. Mater. Sci. Eng. 529 (2019) 012020. https://doi.org/10.1088/1757-899X/529/1/012020.

[8] J. Xu, T. Yang, Z. Li, X. Wang, Y. Xiao, Z. Jian, The recalescence rate of cooling curve for undercooled solidification, Sci. Rep. 10 (2020) 1380. https://doi.org/10.1038/s41598-019-56079-6.

[9] M.C. Flemings, Coarsening in Solidification Processing, Mater. Trans. 46 (2005) 895–900. https://doi.org/10.2320/matertrans.46.895.

[10] D. Ruvalcaba, R.H. Mathiesen, D.G. Eskin, L. Arnberg, L. Katgerman, In situ observations of dendritic fragmentation due to local solute-enrichment during directional solidification of an aluminum alloy, Acta Mater. 55 (2007) 4287–4292. https://doi.org/10.1016/j.actamat.2007.03.030.
[11] R.H. Mathiesen, L. Arnberg, P. Bleuet, A. Somogyi, Crystal fragmentation and columnar-to-equiaxed transitions in Al-Cu studied by synchrotron X-ray video microscopy, Metall. Mater. Trans. A. 37 (2006) 2515–2524. https://doi.org/10.1007/BF02586224.
[12] T. Campanella, C. Charbon, M. Rappaz, Grain refinement induced by electromagnetic stirring: A dendrite fragmentation criterion, Metall. Mater. Trans. A. 35 (2004) 3201–3210. https://doi.org/10.1007/s11661-004-0064-1.
[13] E. Liotti, A. Lui, S. Kumar, Z. Guo, C. Bi, T. Connolley, P.S. Grant, The spatial and temporal distribution of dendrite fragmentation in solidifying Al-Cu alloys under different conditions, Acta Mater. 121 (2016) 384–395. https://doi.org/10.1016/j.actamat.2016.09.013.
[14] X. Li, A. Gagnoud, Y. Fautrelle, Z. Ren, R. Moreau, Y. Zhang, C. Esling, Dendrite fragmentation and columnar-to-equiaxed transition during directional solidification at lower growth speed under a strong magnetic field, Acta Mater. 60 (2012) 3321–3332. https://doi.org/10.1016/j.actamat.2012.02.019.
[15] G. Zimmermann, C. Pickmann, M. Hamacher, E. Schaberger-Zimmermann, H. Neumann-Heyme, K. Eckert, S. Eckert, Fragmentation-driven grain refinement in directional solidification of AlCu10wt-% alloy at low pulling speeds, Acta Mater. 126 (2017) 236–250. https://doi.org/10.1016/j.actamat.2016.12.063.
[16] N. Shevchenko, H. Neumann-Heyme, C. Pickmann, E. Schaberger-Zimmermann, G. Zimmermann, K. Eckert, S. Eckert, Investigations of fluid flow effects on dendritic solidification: Consequences on fragmentation, macrosegregation and the influence of electromagnetic stirring, IOP Conf. Ser. Mater. Sci. Eng. 228 (2017) 012005. https://doi.org/10.1088/1757-899X/228/1/012005.
[17] S. Ananiev, P. Nikrityuk, K. Eckert, Dendrite fragmentation by catastrophic elastic remelting, Acta Mater. 57 (2009) 657–665. https://doi.org/10.1016/j.actamat.2008.10.004.
[18] B. Billia, N. Bergeon, H. Nguyen Thi, H. Jamgotchian, J. Gastaldi, G. Grange, Cumulative Mechanical Moments and Microstructure Deformation Induced by Growth Shape in Columnar Solidification, Phys. Rev. Lett. 93 (2004) 126105. https://doi.org/10.1103/PhysRevLett.93.126105.
[19] G. Reinhart, H. Nguyen-Thi, N. Mangelinck-Noël, J. Baruchel, B. Billia, In Situ Investigation of Dendrite Deformation During Upward Solidification of Al-7wt.%Si, JOM. 66 (2014) 1408–1414. https://doi.org/10.1007/s11837-014-1030-z.
[20] H. Jung, N. Mangelinck-Noël, H. Nguyen-Thi, N. Bergeon, B. Billia, A. Buffet, G. Reinhart, T. Schenk, J. Baruchel, Fragmentation in an Al–7 wt-%Si alloy studied in real time by X-ray synchrotron techniques, Int. J. Cast Met. Res. 22 (2009) 208–211. https://doi.org/10.1179/136404609X367731.
[21] G. Salloum-Abou-Jaoude, H. Nguyen-Thi, G. Reinhart, R.H. Mathiesen, G. Zimmermann, D. Voss, Characterization of Motion of Dendrite Fragment by X-Ray Radiography on Earth and under Microgravity Environment, Mater. Sci. Forum. 790–791 (2014) 311–316. https://doi.org/10.4028/www.scientific.net/MSF.790-791.311.
[22] S. Akamatsu, H. Nguyen-Thi, In situ observation of solidification patterns in diffusive conditions, Acta Mater. 108 (2016) 325–346. https://doi.org/10.1016/j.actamat.2016.01.024.
[23] B. Cai, J. Wang, A. Kao, K. Pericleous, A.B. Phillion, R.C. Atwood, P.D. Lee, 4D synchrotron X-ray tomographic quantification of the transition from cellular to dendrite growth during directional solidification, Acta Mater. 117 (2016) 160–169.

https://doi.org/10.1016/j.actamat.2016.07.002.
[24] T. Nelson, B. Cai, N. Warnken, P.D. Lee, E. Boller, O.V. Magdysyuk, N.R. Green, Gravity effect on thermal-solutal convection during solidification revealed by four-dimensional synchrotron imaging with compositional mapping, Scr. Mater. 180 (2020) 29–33. https://doi.org/10.1016/j.scriptamat.2019.12.026.
[25] K.S. Cruz, E.S. Meza, F.A.P. Fernandes, J.M.V. Quaresma, L.C. Casteletti, A. Garcia, Dendritic Arm Spacing Affecting Mechanical Properties and Wear Behavior of Al-Sn and Al-Si Alloys Directionally Solidified under Unsteady-State Conditions, Metall. Mater. Trans. A. 41 (2010) 972–984. https://doi.org/10.1007/s11661-009-0161-2.
[26] K.S. Cruz, J.E. Spinelli, I.L. Ferreira, N. Cheung, A. Garcia, Microstructural development in Al–Sn alloys directionally solidified under transient heat flow conditions, Mater. Chem. Phys. 109 (2008) 87–98. https://doi.org/10.1016/j.matchemphys.2007.10.037.
[27] R. Nadella, D.G. Eskin, Q. Du, L. Katgerman, Macrosegregation in direct-chill casting of aluminium alloys, Prog. Mater. Sci. 53 (2008) 421–480. https://doi.org/10.1016/j.pmatsci.2007.10.001.
[28] A. Buffet, G. Reinhart, T. Schenk, H. Nguyen-Thi, J. Gastaldi, N. Mangelinck-Noël, H. Jung, J. Härtwig, J. Baruchel, B. Billia, Real-time and in situ solidification of Al-based alloys investigated by synchrotron radiation: a unique experimental set-up combining radiography and topography techniques, Phys. Status Solidi A. 204 (2007) 2721–2727. https://doi.org/10.1002/pssa.200675670.
[29] B. Billia, H. Nguyen-Thi, N. Mangelinck-Noel, N. Bergeon, H. Jung, G. Reinhart, A. Bogno, A. Buffet, J. Hartwig, J. Baruchel, T. Schenk, In Situ Synchrotron X-ray Characterization of Microstructure Formation in Solidification Processing of Al-based Metallic Alloys, ISIJ Int. 50 (2010) 1929–1935. https://doi.org/10.2355/isijinternational.50.1929.
[30] A. Bogno, H. Nguyen-Thi, G. Reinhart, B. Billia, J. Baruchel, Growth and interaction of dendritic equiaxed grains: In situ characterization by synchrotron X-ray radiography, Acta Mater. 61 (2013) 1303–1315. https://doi.org/10.1016/j.actamat.2012.11.008.
[31] A. Bogno, H. Nguyen-Thi, A. Buffet, G. Reinhart, B. Billia, N. Mangelinck-Noël, N. Bergeon, J. Baruchel, T. Schenk, Analysis by synchrotron X-ray radiography of convection effects on the dynamic evolution of the solid–liquid interface and on solute distribution during the initial transient of solidification, Acta Mater. 59 (2011) 4356–4365. https://doi.org/10.1016/j.actamat.2011.03.059.
[32] H. Nguyen-Thi, L. Salvo, R.H. Mathiesen, L. Arnberg, B. Billia, M. Suery, G. Reinhart, On the interest of synchrotron X-ray imaging for the study of solidification in metallic alloys, Comptes Rendus Phys. 13 (2012) 237–245. https://doi.org/10.1016/j.crhy.2011.11.010.
[33] R.H. Mathiesen, L. Arnberg, H. Nguyen-Thi, B. Billia, In Situ X-Ray Video Microscopy as a Tool in Solidification Science, JOM. 64 (2012) 76–82. https://doi.org/10.1007/s11837-011-0213-0.
[34] L. Abou-Khalil, J. Wang, G. Salloum-Abou-Jaoude, M. Garrido, X. Li, Z. Ren, G. Reinhart, H. Nguyen-Thi, Y. Fautrelle, Investigation of Thermo-Electro-Magnetic force on equiaxed grain motion during upward directional solidification, Int. J. Therm. Sci. 145 (2019) 106047. https://doi.org/10.1016/j.ijthermalsci.2019.106047.
[35] A.G. Murphy, W.U. Mirihanage, D.J. Browne, R.H. Mathiesen, Equiaxed dendritic solidification and grain refiner potency characterised through in situ X-radiography, Acta Mater. 95 (2015) 83–89. https://doi.org/10.1016/j.actamat.2015.04.060.
[36] A. Buffet, H. Nguyen-Thi, A. Bogno, T. Schenk, N. Mangelinck-Noël, G. Reinhart, N. Bergeon, B. Billia, J. Baruchel, Measurement of Solute Profiles by Means of Synchrotron X-Ray Radiography during Directional Solidification of Al-4 wt% Cu Alloys, Mater. Sci.

Forum. 649 (2010) 331–336. https://doi.org/10.4028/www.scientific.net/MSF.649.331.
[37] M. Becker, S. Klein, F. Kargl, In-situ solute measurements with a laboratory polychromatic microfocus X-ray source during equiaxed solidification of an Al-Ge alloy, Scr. Mater. 124 (2016) 34–37. https://doi.org/10.1016/j.scriptamat.2016.06.032.
[38] J.W. Rutter, B. Chalmers, A PRISMATIC SUBSTRUCTURE FORMED DURING SOLIDIFICATION OF METALS, Can. J. Phys. 31 (1953) 15–39. https://doi.org/10.1139/p53-003.
[39] W.A. Tiller, K.A. Jackson, J.W. Rutter, B. Chalmers, The redistribution of solute atoms during the solidification of metals, Acta Metall. 1 (1953) 428–437. https://doi.org/10.1016/0001-6160(53)90126-6.
[40] W.W. Mullins, R.F. Sekerka, Stability of a Planar Interface During Solidification of a Dilute Binary Alloy, J. Appl. Phys. 35 (1964) 444–451. https://doi.org/10.1063/1.1713333.
[41] Y.Z. Li, N. Mangelinck-Noël, G. Zimmermann, L. Sturz, H. Nguyen-Thi, Modification of the microstructure by rotating magnetic field during the solidification of Al-7 wt.% Si alloy under microgravity, J. Alloys Compd. 836 (2020) 155458. https://doi.org/10.1016/j.jallcom.2020.155458.
[42] S. Ganesan, D.R. Poirier, Densities of aluminum-rich aluminum-copper alloys during solidification, Metall. Trans. - Phys. Metall. Mater. Sci. 18A (1987) 721–723.
[43] G. Reinhart, A. Buffet, H. Nguyen-Thi, B. Billia, H. Jung, N. Mangelinck-Noël, N. Bergeon, T. Schenk, J. Härtwig, J. Baruchel, In-Situ and Real-Time Analysis of the Formation of Strains and Microstructure Defects during Solidification of Al-3.5 Wt Pct Ni Alloys, Metall. Mater. Trans. A. 39 (2008) 865–874. https://doi.org/10.1007/s11661-007-9449-2.
[44] R.H. Mathiesen, L. Arnberg, Stray crystal formation in Al–20wt.% Cu studied by synchrotron X-ray video microscopy, Mater. Sci. Eng. A. 413–414 (2005) 283–287. https://doi.org/10.1016/j.msea.2005.08.160.
[45] S. Liu, S.-Z. Lu, A. Hellawell, Dendritic array growth in the systems NH4Cl–H2O and [CH2 CN]2–H2O: the detachment of dendrite side arms induced by deceleration, J. Cryst. Growth. 234 (2002) 740–750. https://doi.org/10.1016/S0022-0248(01)01680-3.
[46] H. Neumann-Heyme, K. Eckert, C. Beckermann, Dendrite fragmentation in alloy solidification due to sidearm pinch-off, Phys. Rev. E. 92 (2015) 060401. https://doi.org/10.1103/PhysRevE.92.060401.